Functionalized Boron Nanosheets with Near-Infrared triggered Photothermal and Nitric Oxide Release Activities for Efficient Antibacterial Treatment and Wound Healing Promotion

Jialin Lv,[a] Ye Qi,[a] Yiming Tian,[a] Guangyao Wang [a], Lei Shi[a], Guiling Ning *[a,b] and Junwei Ye,*[a,b]

[a] State Key Laboratory of Fine Chemicals, School of Chemical Engineering, Dalian University of Technology, 2 Linggong Road, Dalian, Liaoning, 116024, P. R. China.

[b] Engineering Laboratory of Boric and Magnesic Functional Material Preparative and Applied Technology, 2 Linggong Road, Dalian, Liaoning, 116024, P. R. China

E-mail: junweiye@dlut.edu.cn, ninggl@dlut.edu.cn

Experimental section

1. Materials

All commercial reagents were of analytical grade and were used without further purification. B powder, Glycidyltrimethylammonium chloride, N,N'-bis-sec-butylamino-p-phenylenediamine (BPA) was purchased from Aladdin Co., Ltd (Shanghai, China). N-Methyl pyrrolidone was purchased from JDTZ Precision Chemical Reagent Factory (Tianjin, China). Chitosan (90% deacetylation) was purchased from Sinopharm chemical Reagent Co., Ltd (Shanghai, China). Sodium nitrite ($NaNO_2$) were provided by Tianjin Damao Chemical Reagent Co., Ltd (Tianjin, China).Ethanol (C_2H_5OH) was obtained from Tianda Chemical Reagent Co., Ltd (Tianjin, China).

2. Characterizations

Contact angle measurements were obtained using an JC2000D2 measuring device. The morphology of the products was characterized using a transmission electron microscopy (TEM) and a high resolution transmission electron microscopy (HRTEM) (Thermo Scientific Tecnai G^2 F30 S-Twin). The Size and thickness of nanosheets were examined by atomic force microscope (AFM) (Dimension Icon, Bruker, USA) X-ray photoelectron spectrometry (XPS) was carried out on a Thermo ESCALAB XI + X-ray photoelectron spectrometer by using an Al Kα source. Powder X-ray diffraction (XRD) data were recorded on a Rigaku D-Max 2400 diffractometer working in reflection mode (Cu-Kα radiation, scanning range 5° to 80°, scanning speed 8° min^{-1}). The size and surface charge (zeta potential) of B NSs were determined using Dynamic Light

Scattering (DLS) (incident beam of 633 nm; ZS90). Thermogravimetric analysis (TGA) was performed on a PerkinElmer TGA/DSC3+ instrument from 30 °C to 800 °C with a heating rate of 10 °C min^{-1} under an air atmosphere. The Fourier transform infrared (FT-IR) spectrum were obtained using KBr pellets method in the range of 4000–400 cm^{-1} on a Perkin-Elmer Jasco 4100 FT-IR spectrometer. UV-vis spectra were measured on sample suspensions using a HITACHI U-4100 UV–Vis spectrophotometer over 200–800 nm. The temperature change was recorded by an infrared thermal camera (FLIR-E60). Fluorescence microscopy (OLYMPUS BX51) was used for the cell wall/membrane integrity assay of the bacteria. The morphologies of the bacteria were investigated using scanning electron microscopy (Tescan Vega3).

3. Photothermal conversion efficiency of B-QCS-BNN6

Following the previous report, The detailed calculation is shown as follow[R1]:

the energy balance for the whole system is

$$\sum_i m_i C_{pi} \frac{dT}{dt} = Q_{Sample} + Q_s - Q_{Loss} \quad (1)$$

where C_{pi} and m_i are the heat capacity and the mass of solvent (water), T is the solution temperature, Q_{sample} is the energy input of B-QCS-BNN6, Q_s is the baseline energy input of the sample cell, and Q_{Loss} is the heat conducted away from the system surface by air.

The NIR laser-induced source term, B-QCS-BNN6, expresses heat dissipated under the irradiation of an 808 nm laser

$$Q_{Sample} = I(1 - 10^{-A_{808}})\eta \quad (2)$$

where I is the incident energy of the NIR laser (W), A_{808} is the absorbance of the B-QCS-BNN6 at the NIR laser of 808 nm, and η is the photothermal-conversion efficiency from the incident NIR laser energy to thermal energy. Besides, Q_S is temperature-dependent parameter, which is linear with the output of thermal energy.

$$Q_{Loss} = hA\Delta T \qquad (3)$$

where h represents heat-transfer coefficient, A represents the surface area of the container, ΔT represents the temperature difference between system surface and the surrounding temperature. Since the heat output (Q_{Loss}) is increased along with the rise in temperature according to eq 3, the temperature of system will reach a maximum when the heat output is equal to heat input

$$Q_{Sample} + Q_s = Q_{Loss} = hA\Delta T_{max} \qquad (4)$$

where $hA\Delta T_{max}$ represents conducting heat away from the system surface by air when the sample cell reaches the equilibrium temperature. The photothermal conversion efficiency (η) can be obtained by substituting eq 2 into eq 4 and rearranging to get

$$\eta = \frac{hA\Delta T_{max}}{I(1 - 10^{-A_{808}})} \qquad (5)$$

where A is the absorbance of B-QCS-BNN6 at λ of 808 nm. Thus, only the hA remains unknown for the calculation of η

In order to obtain hA, a dimensionless driving force temperature, θ, is introduced and scaled using the maximum system temperature,

$$\theta = \frac{\Delta T}{\Delta T_{max}} \qquad (6)$$

and a time constant of sample system, *t*

$$t = -\frac{\sum_i m_i C_{pi}}{hA}\theta \quad (7)$$

which is substituted into eq 1 and rearranged to yield

$$\frac{d\theta}{dt} = \frac{hA}{\sum_i m_i C_{pi}}[\frac{Q_{Sample} + Q_s}{hA\Delta T_{max}} \quad (8)$$

At the cooling period of B-QCS-BNN6 dispersion, the laser radiation ceases and Q_{sample} + Q_s = 0, reducing eq 8 to

$$dt = -\frac{\sum_i m_i C_{pi}}{hA}\frac{d\theta}{\theta} \quad (9)$$

$$\tau_s = -\frac{\sum_i m_i C_{pi}}{hA} \quad (10)$$

For B-QCS-BNN6, the τ_s=164.24 s, m is 0.2 g and C is 4.2 J/g, hA can be calculated to 0.0051145 W/^{o}C. Subsitituting *I*=2 W/cm^2, A_{808}=0.218, $\triangle T_{max}$=34.002 ^{o}C into Eq (5), the 808 nm laser photothermal conversion efficiency (η) of B-QCS-BNN6 can be calculated to be 22.03%.

Reference

[R1] X. Ji, N. Kong, J. Wang, W. Li, Y. Xiao, S. T. Gan, Y. Zhang, Y. Li, X. Song, Q. Xiong, S. Shi, Z. Li, W. Tao, H. Zhang, L. Mei and J. Shi, *Adv Mater*, 2018, **30**, e1803031.

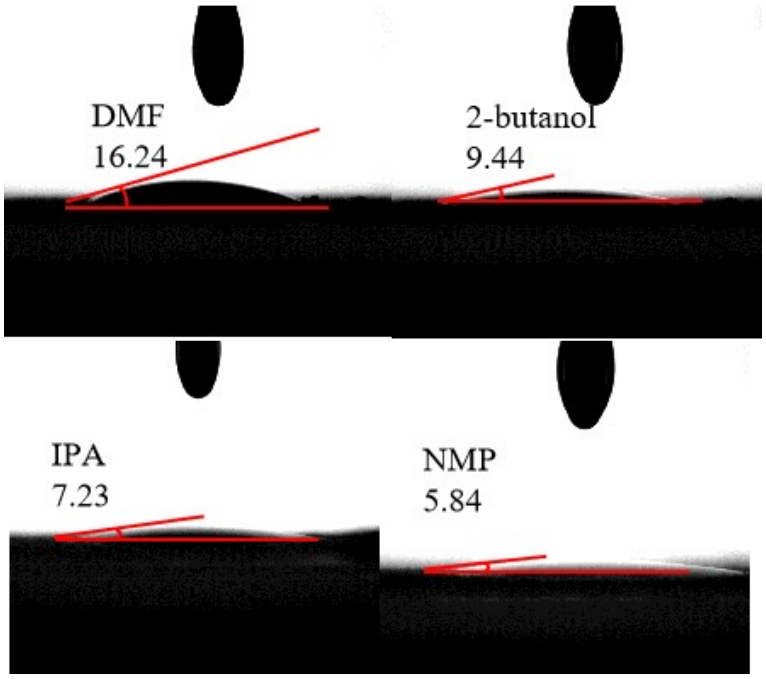

Fig. S1 Contact Angle of boron powder with different solvents.

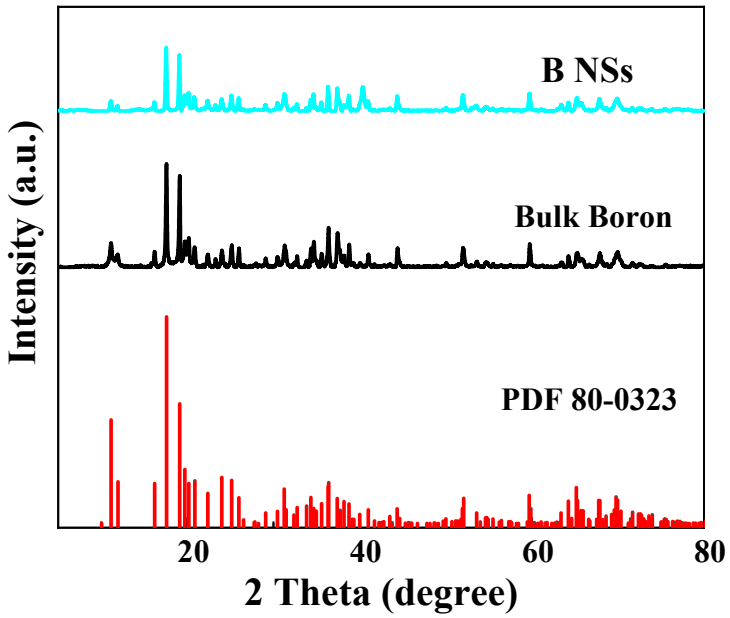

Fig. S2 XRD patterns of boron powder and B NSs.

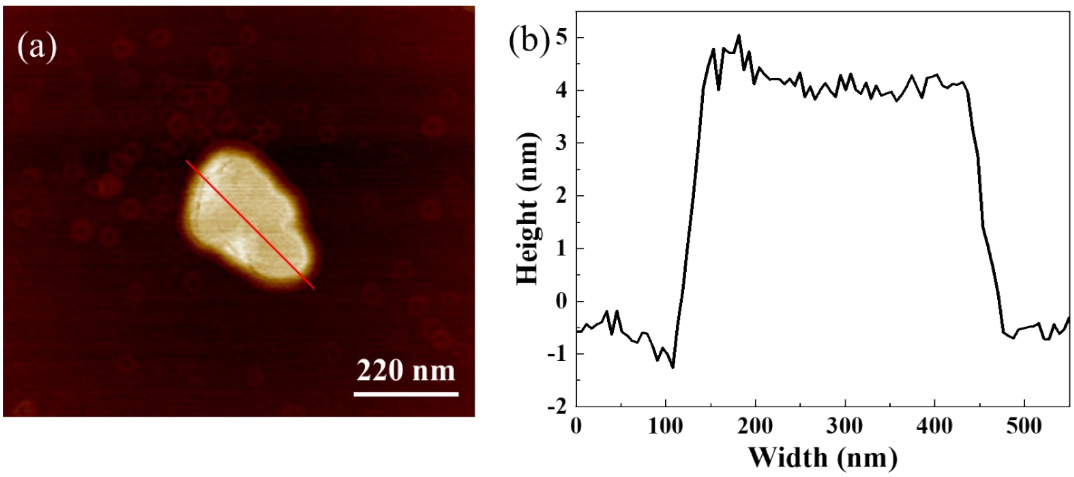

Fig. S3 AFM image of boron nanosheets after coated with QCS (B-QCS)

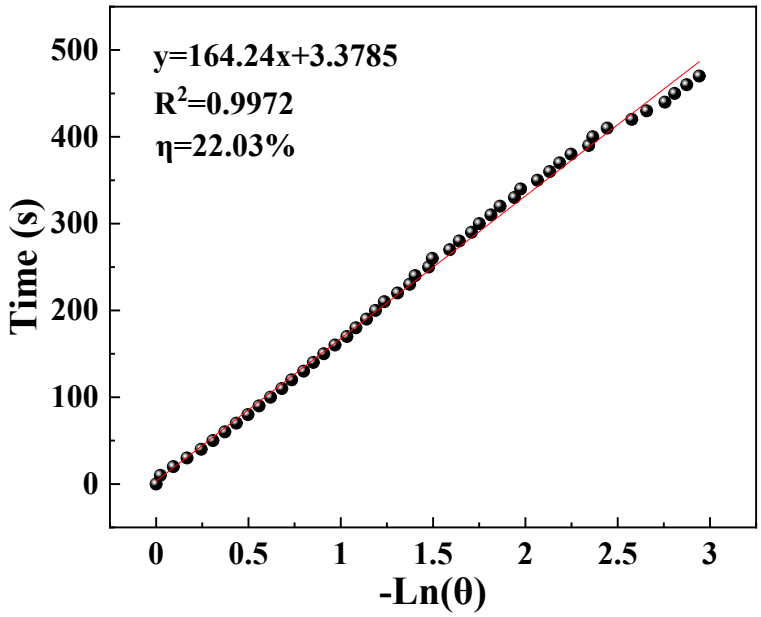

Fig. S4 Linear time data versus -ln(θ) acquired from the cooling period of panel

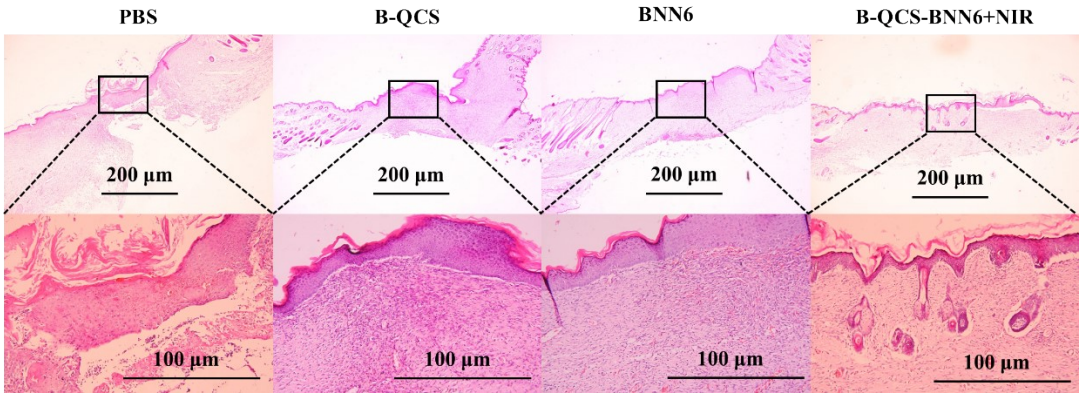

Fig. S5 H&E trichrome staining of skin tissues in wound sites at time points of 14 day.

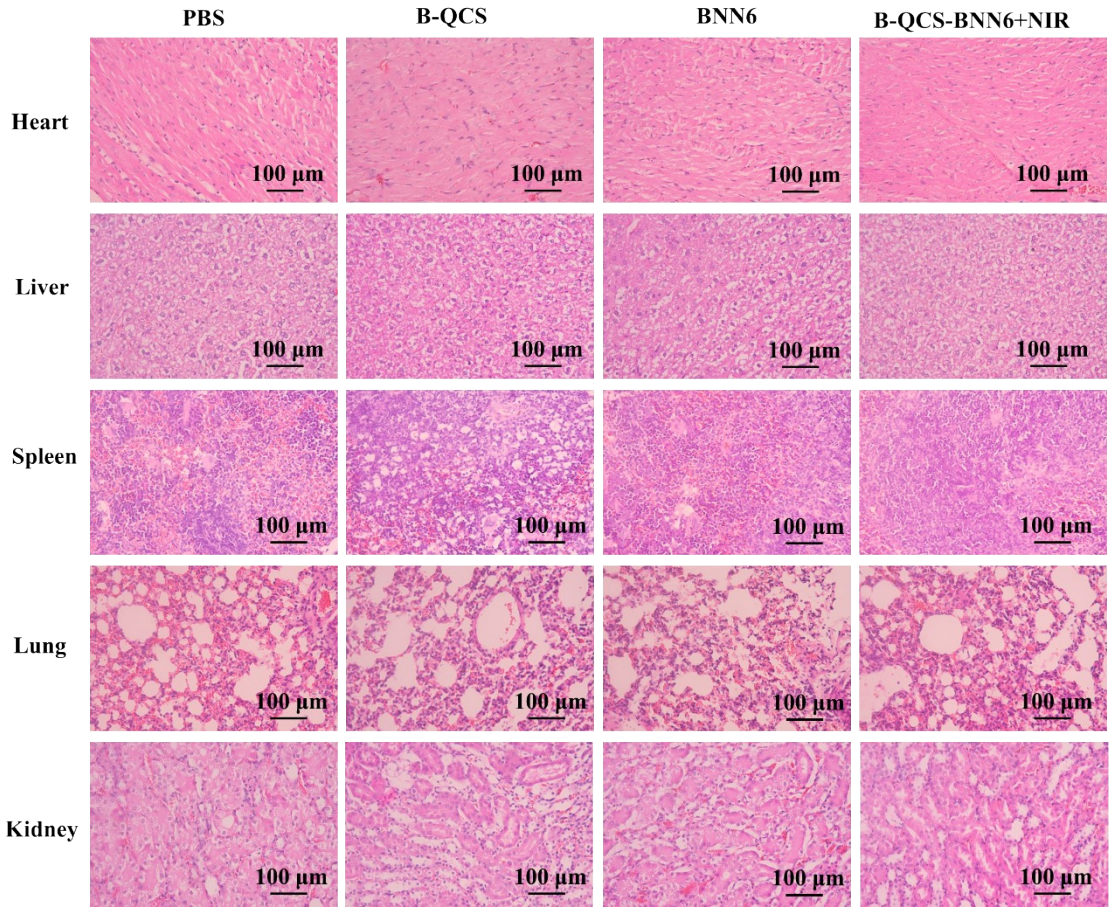

Fig. S6 H&E staining of the main organs (heart, liver, spleen, lung, kidney) of the mice received different treatments at day 14.